Supporting Information

Accelerated selective oxidation of benzyl alcohol to benzaldehyde via a self-catalyzed Pickering emulsion microreactor

Hongbing Dan [a,b], Han Zhao [a], Yue Gao [a,*], Baiyu Zhang [b], Xing Xu [a], Qinyan Yue [a], Tiina Leiviskä [c], Bo Jin [d], Bing Chen [b] and Baoyu Gao [a]

a. *Shandong Provincial Key Laboratory of Water Pollution Control and Resource Reuse, School of Environmental Science and Engineering, Shandong University, Jinan 250100, PR China*

b. *Northern Region Persistent Organic Pollution Control (NRPOP) Laboratory, Faculty of Engineering and Applied Science, Memorial University of Newfoundland, St. John's, NL, A1B 3X5, Canada*

c. *Chemical Process Engineering, University of Oulu, PO Box 4300, FIN-90014, Oulu, Finland*

d. *School of Chemical Engineering, The University of Adelaide, 5005 Adelaide, Australia*

*Corresponding author:

E-mail: ygao@sdu.edu.cn (Y. Gao).

This *Supporting Information* includes

21 Pages

5 Texts

16 Figures

3 Tables

Text S1. Materials

The pristine *Enteromorpha*, collected from the coast in Qingdao, China (36.15 N, 120.58 E), was first rinsed with tap water, dried at 50℃ overnight, and then grounded to powders with a particle size of 50-200 μm. The chemicals, including n-hexane, benzyl alcohol (BzOH), benzaldehyde (BzH), potassium peroxymonosulfate (PMS), tert-butyl alcohol (TBA), ethyl alcohol (EtOH), furfuryl alcohol (FFA), p-benzoquinone (p-BQ) and dimethyl sulfoxide (DMSO), were purchased from Sinopharm Chemical Reagent Co., Ltd (Shanghai, China) and used directly without further purification.

Text S2. Preparation of ESAB

A certain amount of *Enteromorpha* powders was first put into a 10 mL corundum crucible, and then experienced a pyrolysis process in N_2 atmosphere at temperature of 800℃ for 2 h. The heating rate was designed at 5 ℃ min^{-1}. Next, 2 g *Enteromorpha*-derived biochar coupled with 20 mL deionized water were sealed in an agate jar and undergone a ball-milling treatment at a rotate speed of 240 r/min for 300 min. The ball-milled samples were rinsed with deionized water and ethyl alcohol separately to remove impurities. It was then collected after vacuum drying at 50℃ overnight. The ESAB obtained at different pyrolysis temperature (X) is noted as ESAB-X.

Text S3. Characterization of Enteromorpha-prolifera-derived super-amphiphilic biochar

The surface morphologies corresponding elemental compositions of ESAB-800 were identified using a field-emission scanning electron microscopy (SEM, SU8010) equipped with an energy dispersive spectroscopy (EDS) and a transmission electron microscope (JEOL 2100, TEM). High angle annular dark field scanning TEM (HAADF-STEM) images and corresponding elemental mapping were achieved by FEI Titan G2 80-200 TEM/STEM. N_2 adsorption/desorption measurements at -196 ℃ (JW-BK122W, China) were employed to determine the Brunauer-Emmett-Teller (BET) surface area and pore-size distribution of samples. X-ray diffractometer (XRD, Cu Kα, λ = 0.15406 nm, Bruker D8 Advance) at a scanning rate of 5°/min was applied to clarify

the crystal structures of catalysts. The surface functional groups were identified by Fourier transform infrared spectrometer (FTIR, Thermo Scientific, US) at a range of 500-4000 cm^{-1}. Raman spectra of samples were recorded from 250 to 4000 cm^{-1} on a Raman spectrometer (Thermo Fischer DXR). The X-ray photoelectron spectroscopy (XPS) analysis was performed to investigate the surface elemental compositions and chemical states of enteromorpha-prolifera-derived super-amphiphilic biochar (ESAB). The surface wettability of various samples was clarified by a contact angle tester (HARKE-SPCAX1S). The particle size distribution of Pickering emulsion was identified by using an optical microscope (XSP-8CA).

Text S4. Electrochemical performance measurements

All the electrochemical tests were carried out at room temperature on a CHI 760E electrochemical workstation (Shanghai Chenhua Instruments Inc., China), equipped with a standard three-electrode electrolytic cell using 0.5 M Na_2SO_4 aqueous solution as electrolyte. Pt foil and saturated Ag/AgCl electrodes were set as a counter electrode and a reference electrode, respectively.

The working electrodes were prepared via the following procedure, based on the previously published methods [1, 2]. (i) Glassy carbon electrode was firstly polished repeatedly by employing Al_2O_3, and then cleaned up and dried by N_2 blowing. (ii) 5.0 mg of catalyst, 40 μL of Nafion (5 wt %) and 1 mL of N,N-dimethylformamide were mixed evenly via sonication for 1 h. (iii) 3 μL of suspensions was dropped onto the clean glassy carbon electrode and air-dried in the ambient environment. Electrochemical impedance spectra (EIS) were recorded at −0.3 V *vs*. Ag/AgCl within a frequency range from 10^6 to 10^{-1} Hz using an AC voltage at a 5 mV amplitude.

Text S5. Galvanic oxidation system

In a galvanic oxidation system, the catalyst ink (5 mg ESAB-800, 40 μL nafion in 1 mL N,N-dimethylformamide) was coated on a 20 × 20 × 3 mm graphite plate for electron channel and adsorption plate for BzOH and PMS. The loading amount of catalyst was about 0.19 mg/cm^2. A copper wire was used to connect the two electrodes

for inter cell electron transfer. The salt bridge was prepared by adding the mixture of 3 g agar and 30 g KCl in 97 ml water into U-shaped glass tube and cool down it to room temperature.

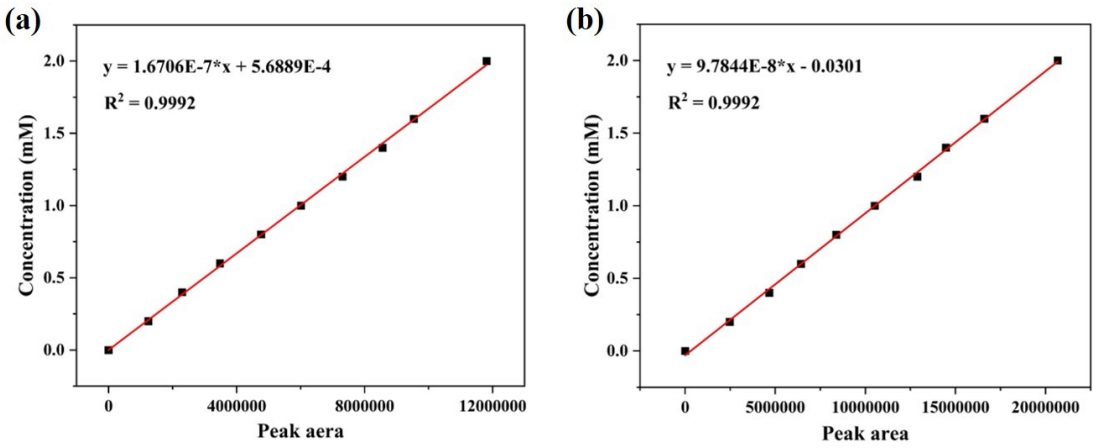

Fig. S1. Calibration curves of benzyl alcohol (a) and benzaldehyde (b).

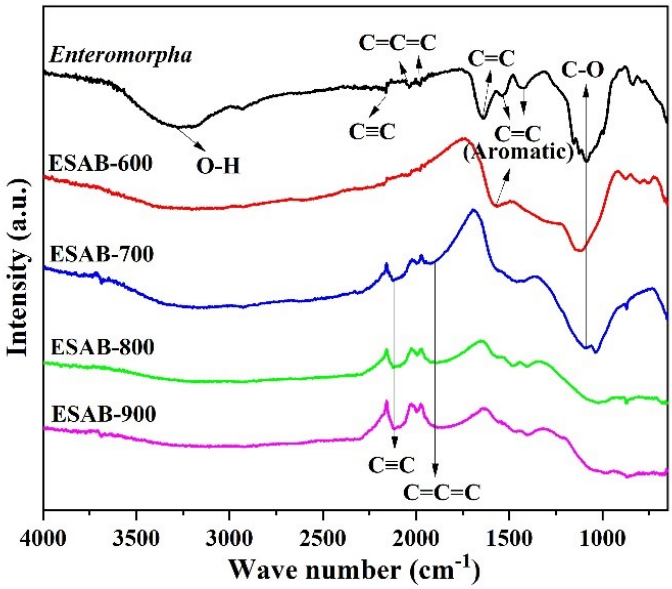

Fig. S2. FTIR spectra of *Enteromorpha*, ESAB-600, ESAB-700, ESAB-800 and ESAB-900.

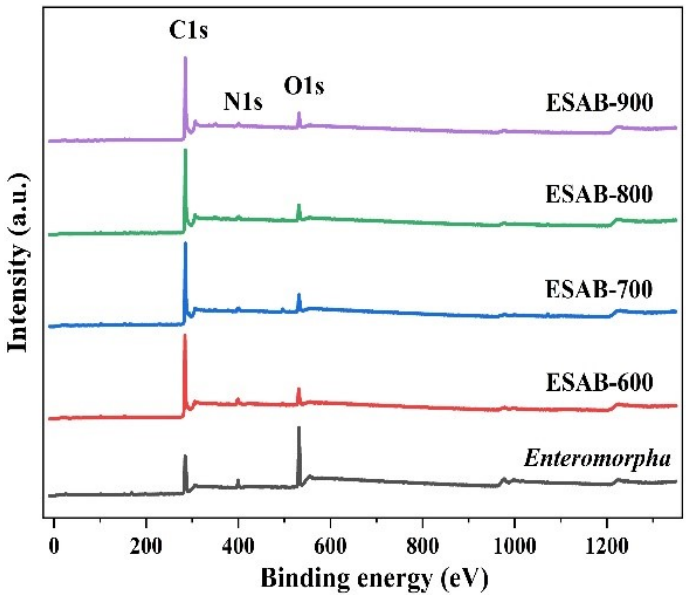

Fig. S3. Survey XPS spectra of *Enteromorpha*, ESAB-600, ESAB-700, ESAB-800 and ESAB-900.

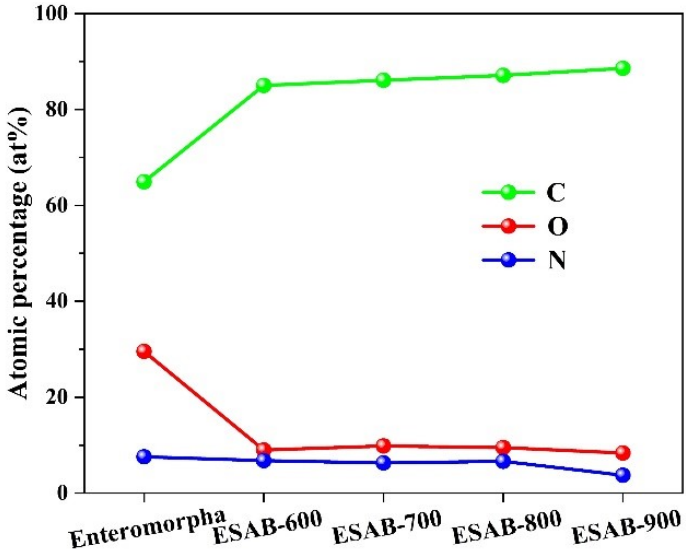

Fig. S4. Atomic percentage (at%) of C, N and O in *Enteromorpha*, ESAB-600, ESAB-700, ESAB-800 and ESAB-900.

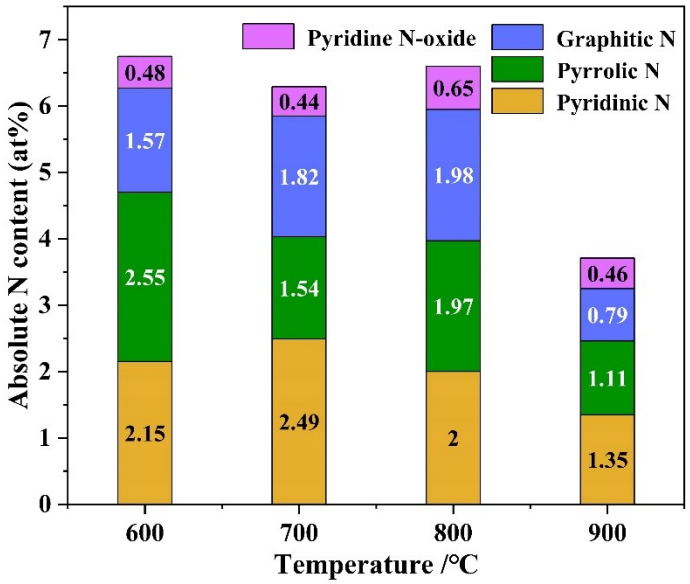

Fig. S5. Absolute contents of pyridinic N, pyrrolic N, graphitic N and pyridine N-oxide in each ESAB by the deconvolution of N1s XPS spectra.

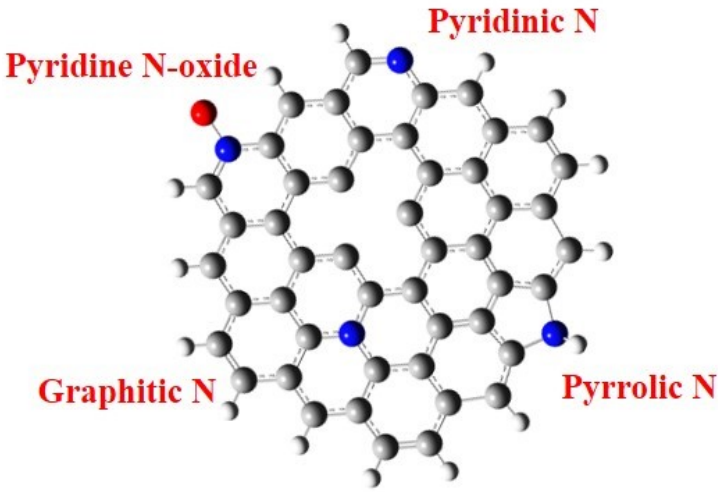

Fig. S6. Schematic illustration of various nitrogen species doped in ESAB, namely, pyridinic N, pyrrolic N, graphitic N and pyridine N-oxide (i).

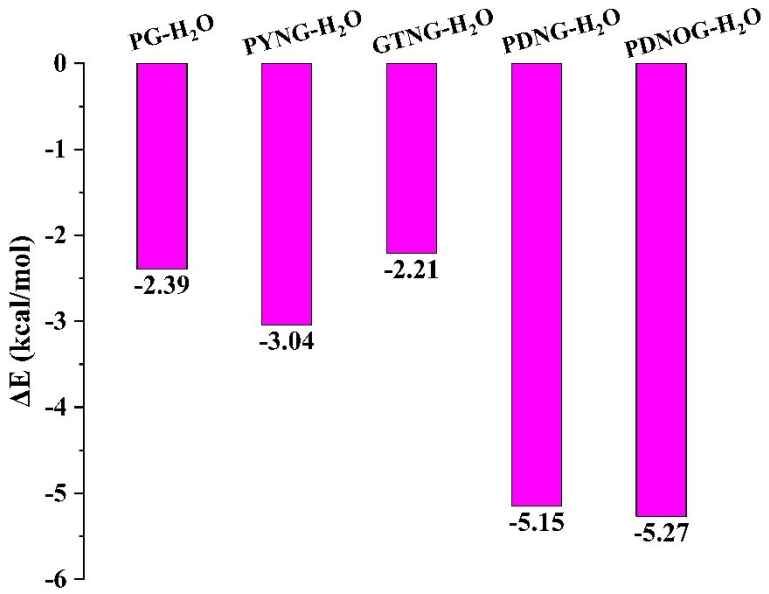

Fig. S7. Adsorption energies (ΔEs) of H_2O to pristine graphene (PG), pyrrolic N-doped graphene (PYNG), graphitic N-doped graphene (GTNG), pyridinic N-doped graphene (PDNG), and pyridine N-oxide-doped graphene (PDNOG).

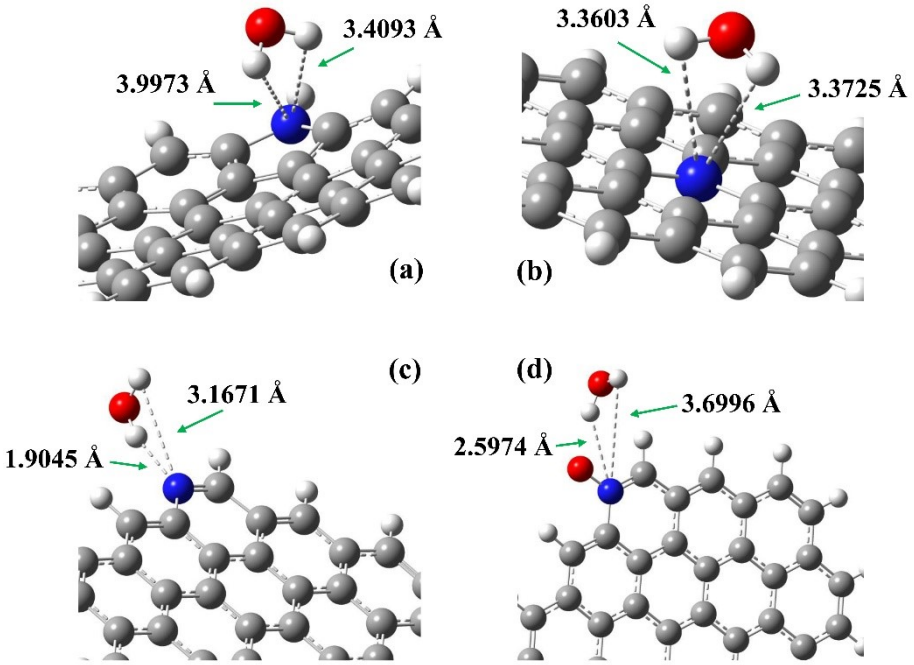

Fig. S8. The distance between H atom in H_2O and N atom in graphene, i.e., OH · · · N. a: pyrrolic N-doped graphene; (b) graphitic N-doped graphene; (c) pyridinic N-doped graphene; (d) oxidized pyridinic N-doped graphene.

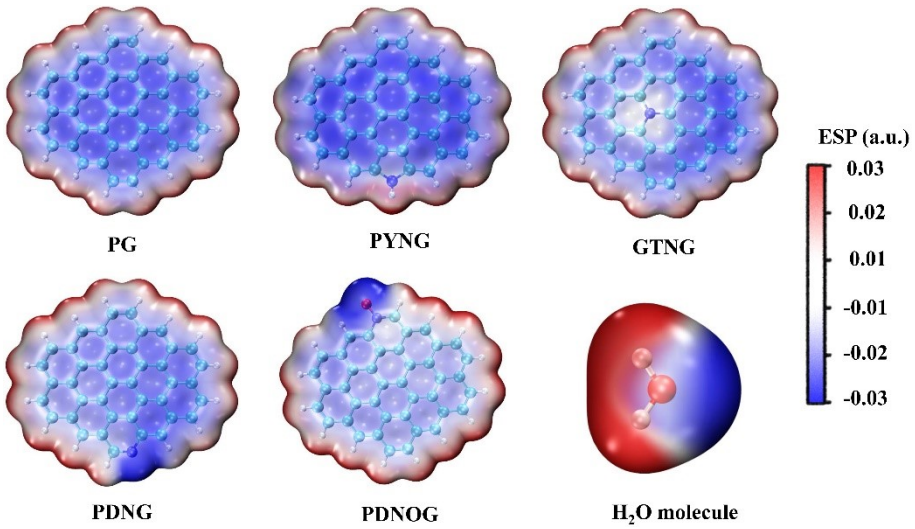

Fig. S9. Distributions of electrostatic potential (ESP) for pristine graphene (PG), pyrrolic N-doped graphene (PYNG), graphitic N-doped graphene (GTNG), pyridinic N-doped graphene (PDNG), oxidized pyridinic N-doped graphene (PDNOG) and H_2O molecule.

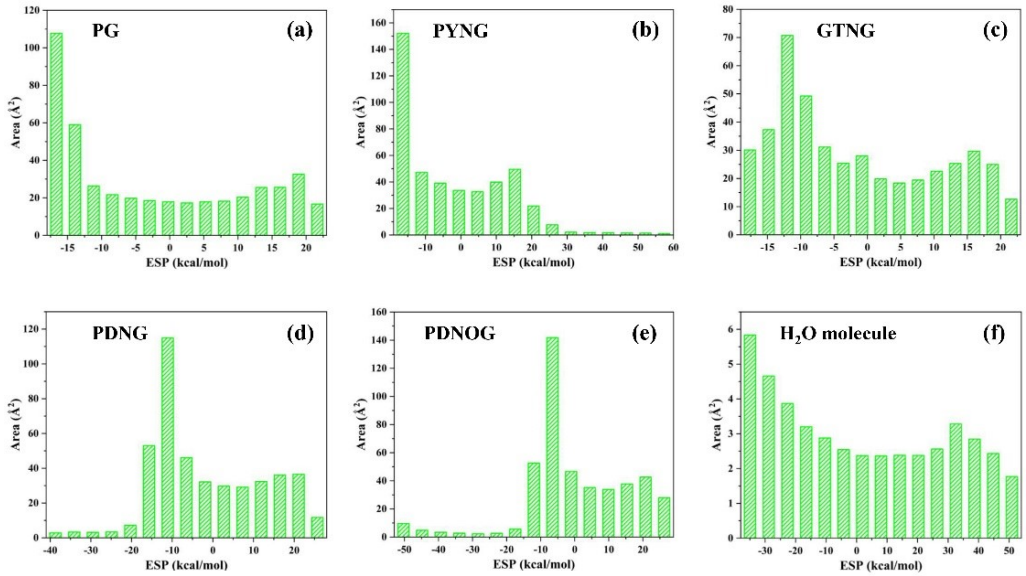

Fig. S10. Surface area in each electrostatic potential (ESP) range on the Van der Waals surface of PG (a), PYNG (b), GTNG (c), PDNG (d), PDNOG (e) and H_2O molecule.

Figs. S9-10 display the electrostatic potential (ESP) distribution of PG, PYNG, GTNG, PDNG, PDNOG and H_2O molecule. It is observed that the incorporation of pyridinic N and pyridinic N-oxide highly improved the local electronegativity of PG. As a result, strong electrostatic attraction interaction can be formed between H atoms in H_2O molecule and pyridinic N (pyridinic N-oxide), thus promoting the water uptake to keep super-hydrophilic.

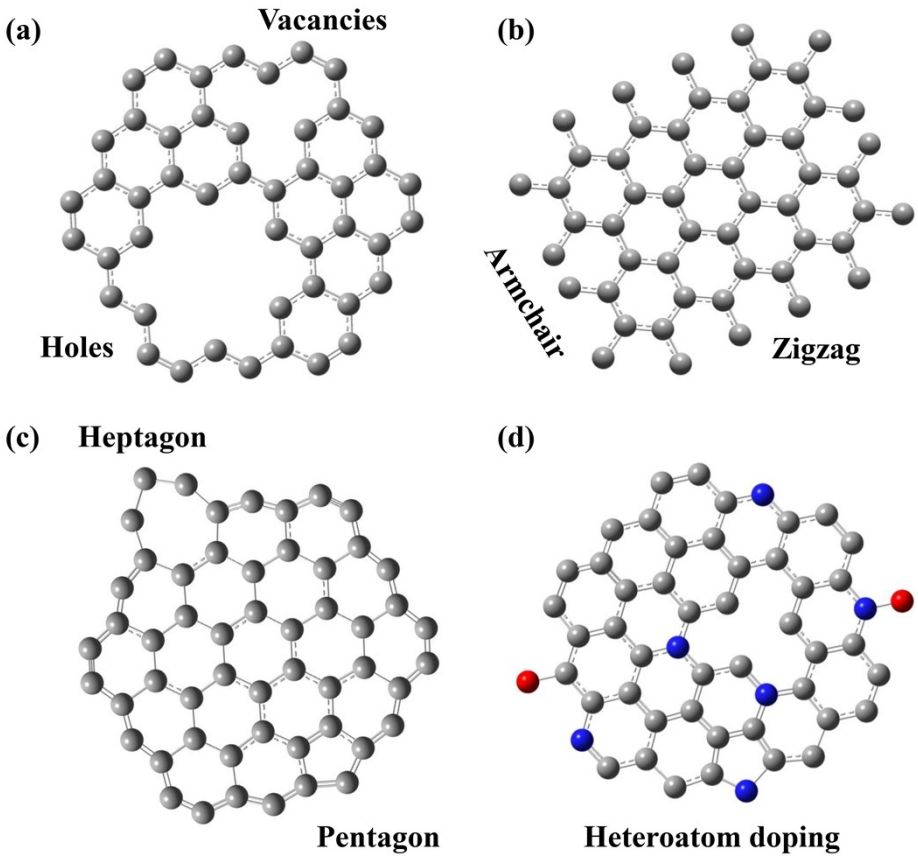

Fig. S11. Schematic diagrams of vacancy and hole defects (a), edge defects (b), topological defects (c), heteroatom doping defects (d) in ESAB.

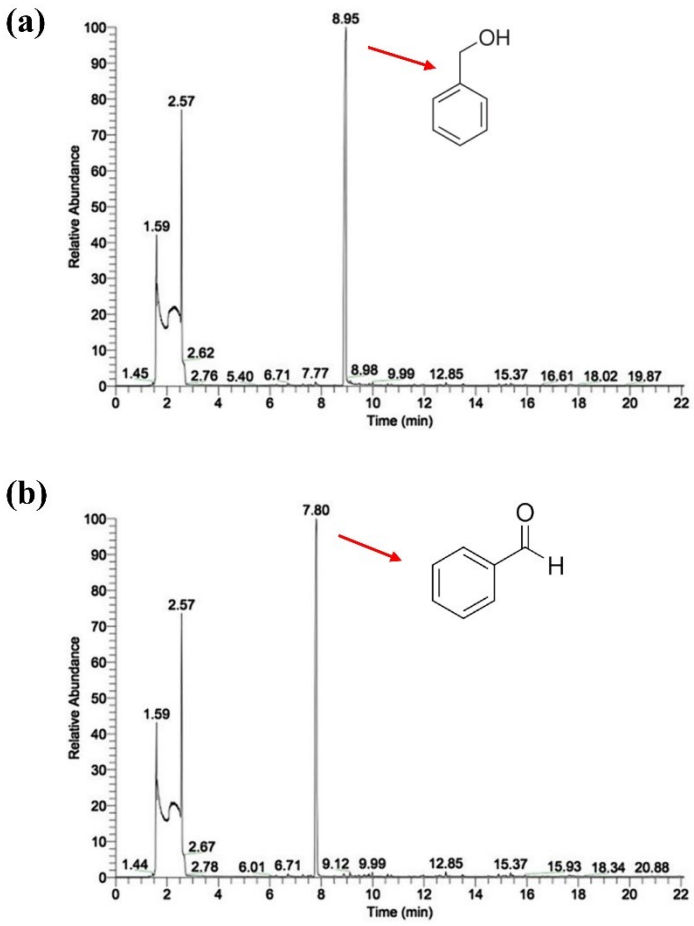

Fig. S12. GC-MS spectra of chromatographically pure benzyl alcohol (a) and benzaldehyde (b).

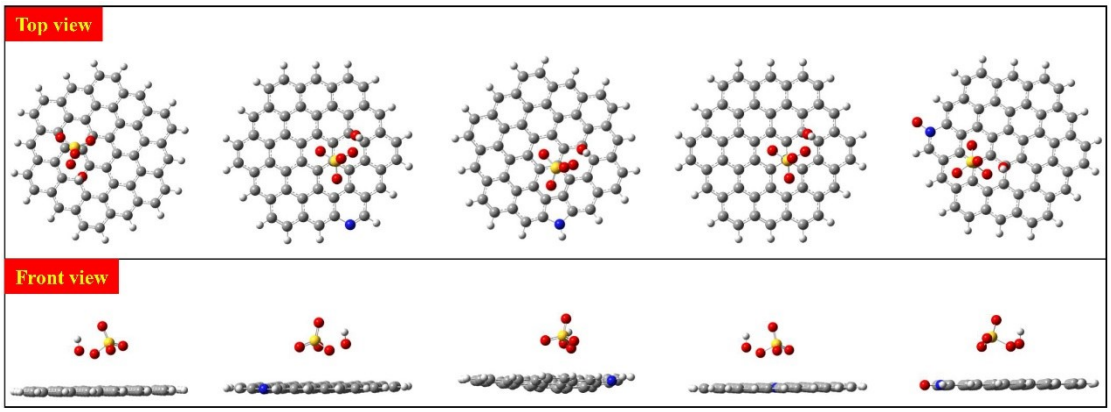

Fig. S13. Optimized binding configurations of PMS with pristine graphene (PG), pyridinic N-doped graphene (PDNG), pyrrolic N-doped graphene (PYNG), graphitic N-doped graphene (GTNG) and pyridine N-oxide-doped graphene (PDNOG), as shown in both top and front views.

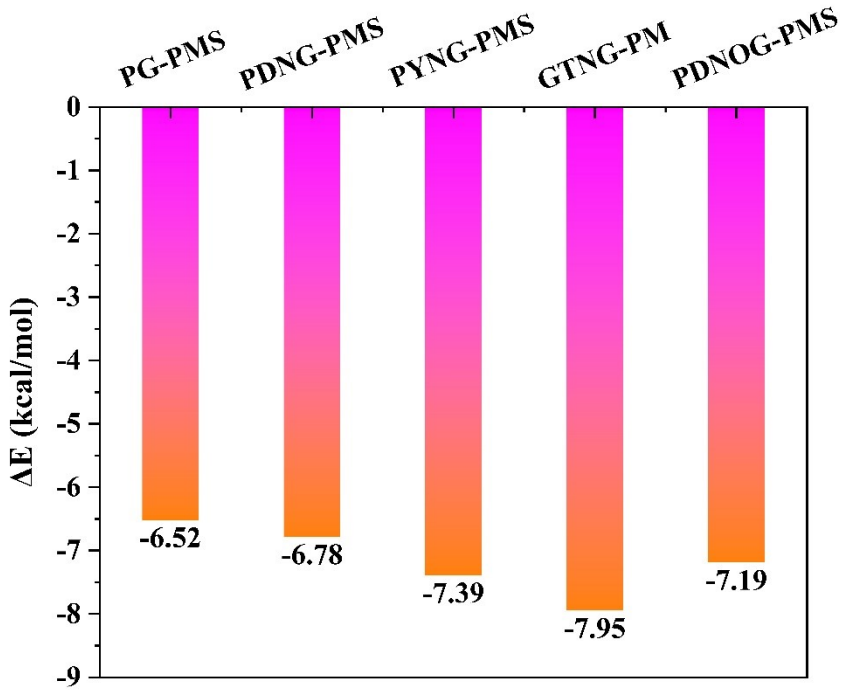

Fig. S14. Adsorption energies (ΔEs) of PMS to pristine graphene (PG), pyridinic N-doped graphene (PDNG), pyrrolic N-doped graphene (PYNG), graphitic N-doped graphene (GTNG) and pyridine N-oxide-doped graphene (PDNOG, g).

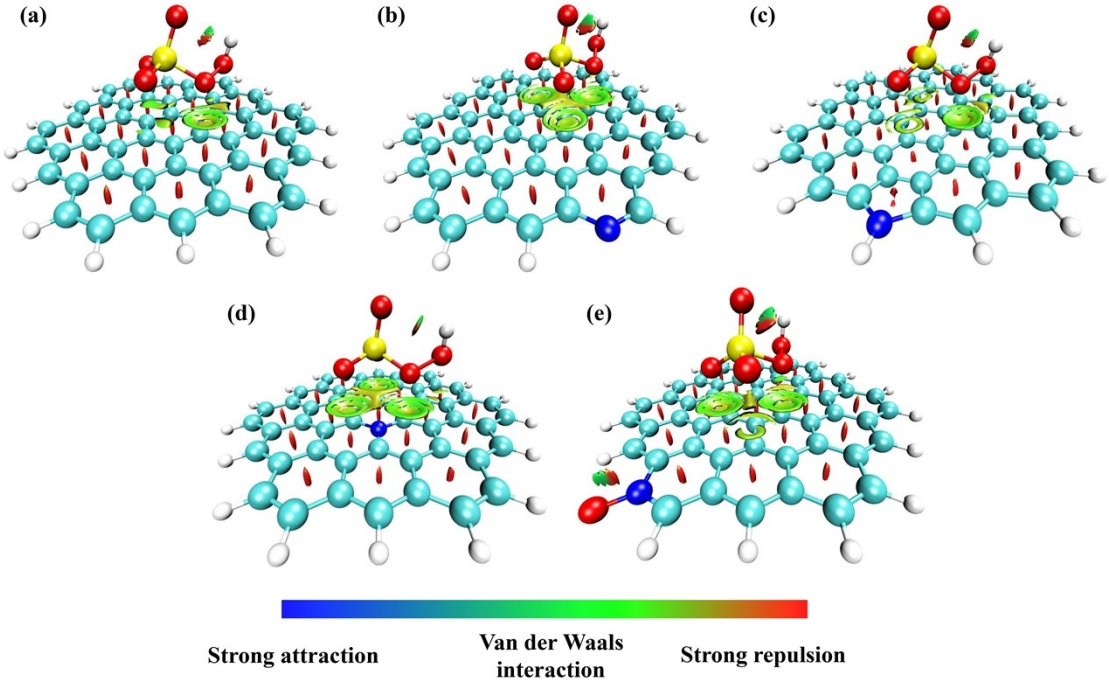

Fig. S15. Reduced density gradient (RDG) isosurfaces (s = 0.5 a.u.) by the values of sign(λ_2)ρ for PG-PMS (a), PDNG-PMS (b), PYNG-PMS (c), GTNG-PMS (d) and PDNOG-PMS (e) systems.

To clarify the specific interaction between PMS and various N-doped graphene fragments, reduced density gradient (RDG) function analysis was further carried out (Fig. S15). For both nitrogen-free and nitrogen-doped graphene sheets, a distinct green region is observed at their interface with PMS molecule, demonstrating the presence of van der Waals forces [3, 4].

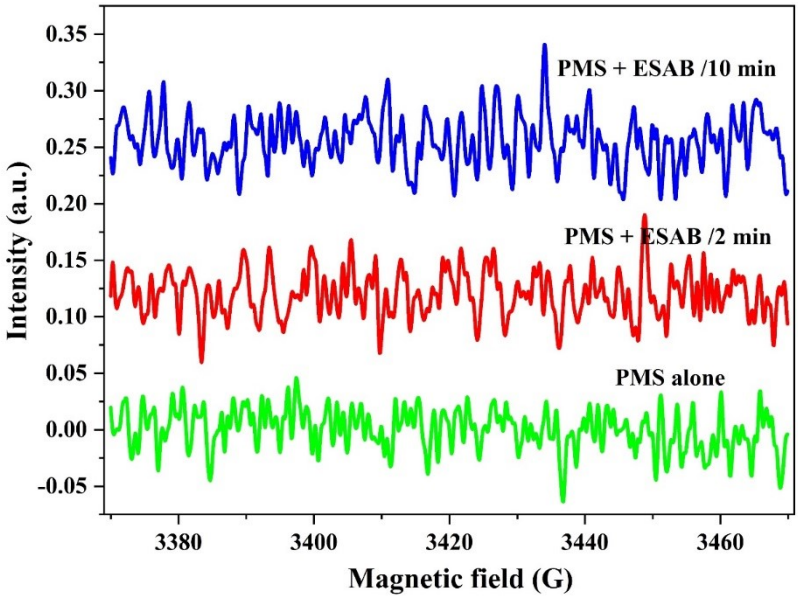

Fig. S16. EPR spectra in PMS/ESAB-800 system using DMPO for capturing $SO_4^{\bullet-}$ and •OH.

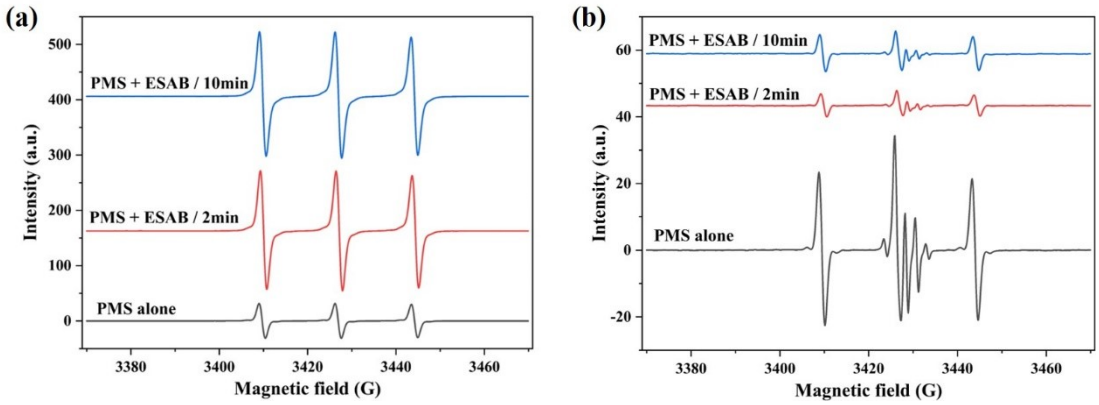

Fig. S17. EPR spectra for TEMP-$^1O_2$: without (a) and with (b) adding *p*-BQ (b).

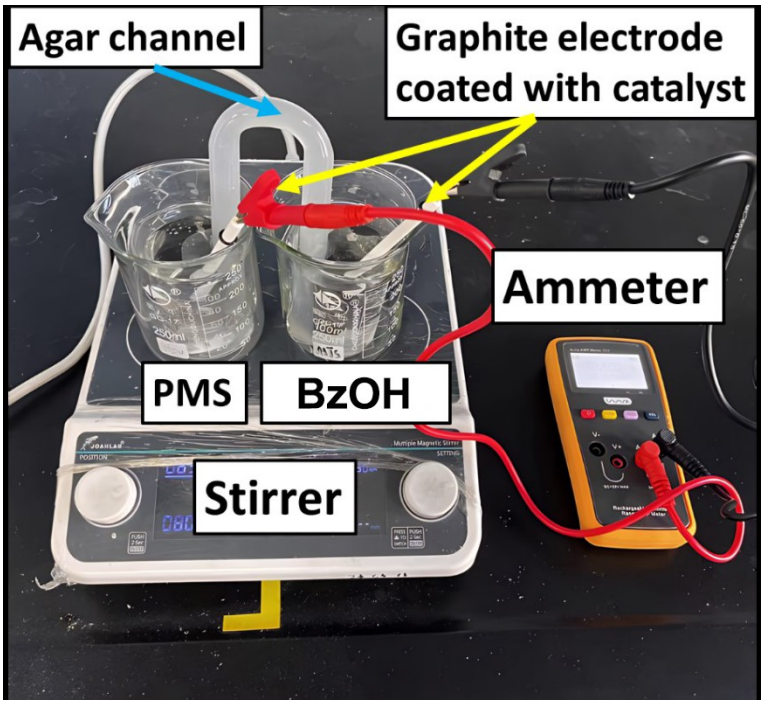

Fig. S18. Digital image of galvanic oxidation system (GOS).

Table S1 UPLC analysis methods for BzOH and BzH.

Samples	Mobile phase	Wavelength (nm)	Flow rate (mL min^{-1})	Column temperature (℃)
BzOH	MeOH/H_2O = 7/3	215	0.8	25
BzH	MeOH/H_2O = 9/1	250	0.8	25

Table S2 The atomic percent of C, N and O in *Enteromorpha*, ESAB-600, ESAB-700, ESAB-800 and ESAB-900.

Sample	C (at%)	N (at%)	O (at%)	C/O ratio
Enteromorpha	64.91	7.56	29.53	2.20
ESAB-600	85.01	6.75	8.98	9.47
ESAB-700	86.09	6.29	9.82	8.77
ESAB-800	87.11	6.61	9.47	9.20
ESAB-900	88.56	3.72	8.34	10.62

Table S3 Surface properties of the as-prepared catalysts.

Samples	BET surface area (m^2 g^{-1})	Total pore volume (cm^3 g^{-1})	Average pore diameter (nm)
ESAB-600	104	0.20	7.926
ESAB-700	100	0.19	7.995
ESAB-800	171	0.21	7.514
ESAB-900	189	0.22	7.081

References

1. Y. N. Shang, X. Xu, Z. H. Wang, B. Jin, R. Wang, Z. F. Ren, B. Y. Gao and Q. Y. Yue, *Acs Sustainable Chemistry & Engineering*, 2018, **6**, 6920-6931.
2. C. Chen, T. F. Ma, Y. N. Shang, B. Y. Gao, B. Jin, H. B. Dan, Q. Li, Q. Y. Yue, Y. W. Li, Y. Wang and X. Xu, *Applied Catalysis B-Environmental*, 2019, **250**, 382-395.
3. C. Li, X. S. Liu, Y. L. Han, Q. Guo, W. B. Yang, Q. Liu, B. Song, X. L. Zheng and S. Y. Tao, *Cell Reports Physical Science*, 2021, **2**.
4. H. Dan, Y. Gao, L. Feng, W. Yin, X. Xu, B. Gao and Q. Yue, *Journal of Hazardous Materials*, 2023, **445**, 130469.